

1 Formation mechanisms of atmospheric nitrate and sulfate during the
2 winter haze pollution periods in Beijing: gas-phase, heterogeneous
3 and aqueous-phase chemistry

4 Pengfei Liu^{1, 2, 3, 5}, Can Ye^{1, 3}, Chaoyang Xue^{1, 3}, Chenglong Zhang^{1, 2, 3}, Yujing Mu^{1, 2, 3, 4}, Xu
5 Sun^{1, 6}

6 ¹ Research Center for Eco-Environmental Sciences, Chinese Academy of Sciences, Beijing, 100085, China.

7 ² Center for Excellence in Urban Atmospheric Environment, Institute of Urban Environment, Chinese Academy of
8 Sciences, Xiamen, 361021, China.

9 ³ University of Chinese Academy of Sciences, Beijing, 100049, China.

10 ⁴ National Engineering Laboratory for VOCs Pollution Control Material & Technology, University of Chinese
11 Academy of Sciences, Beijing, 100049, China.

12 ⁵ Key Laboratory of Atmospheric Chemistry, China Meteorological Administration, Beijing, 100081, China.

13 ⁶ Beijing Urban Ecosystem Research Station, Beijing, 100085, China.

14 **Correspondence: Yujing Mu** (yjmu@rcees.ac.cn)

15 **Abstract**

16 A vast area in China is currently going through severe haze episodes with drastically elevated
17 concentrations of PM_{2.5} in winter. Nitrate and sulfate are main constituents of PM_{2.5} but their
18 formations via NO₂ and SO₂ oxidation are still not comprehensively understood, especially under
19 different pollution or atmospheric relative humidity (RH) conditions. To elucidate formation
20 pathways of nitrate and sulfate in different polluted cases, hourly samples of PM_{2.5} were collected
21 continuously in Beijing during the wintertime of 2016. Three serious pollution cases were
22 identified reasonably during the sampling period and the secondary formations of nitrate and
23 sulfate were found to make a dominant contribution to atmospheric PM_{2.5} under the relatively high
24 RH condition. The significant correlation between NOR (NOR = NO₃⁻ / (NO₃⁻ + NO₂)) and [NO₂]² ×
25 [O₃] during the nighttime under the RH ≥ 60% condition indicated that the heterogeneous
26 hydrolysis of N₂O₅ involving aerosol liquid water was responsible for the nocturnal formation of
27 nitrate at the extremely high RH levels. The more coincident trend of NOR and [HONO] × [DR]

28 (direct radiation) \times $[\text{NO}_2]$ than $[\text{Dust}] \times [\text{NO}_2]$ during the daytime under the 30%<RH<60%
29 condition provided convincing evidence that the gas-phase reaction of NO_2 with OH played a
30 pivotal role in the diurnal formation of nitrate at moderate RH levels. The extremely high mean
31 values of SOR ($\text{SOR} = \text{SO}_4^{2-} / (\text{SO}_4^{2-} + \text{SO}_2)$) during the whole day under the $\text{RH} \geq 60\%$ condition
32 could be ascribed to the evident contribution of SO_2 aqueous-phase oxidation to the formation of
33 sulfate during the severe pollution episodes. Based on the parameters measured in this study and
34 the known sulfate production rate calculation method, the oxidation pathway of H_2O_2 rather than
35 NO_2 was found to contribute greatly to the aqueous-phase formation of sulfate.

36 **1. Introduction**

37 In recent years, severe haze has occurred frequently in Beijing as well as the North China
38 Plain (NCP) during the wintertime, which has aroused great attention from the public due to its
39 adverse impact on atmospheric visibility, air quality and human health (Chan and Yao,
40 2008;Zhang et al., 2012;Zhang et al., 2015).

41 To mitigate the severe haze pollution situations, a series of regulatory measures for primary
42 pollution sources have been implemented by the Chinese government. For example, coal
43 combustion for heating in winter has gradually been replaced with electricity and natural gas in
44 the NCP, coal-fired power plants have been strictly required to install flue-gas denitration and
45 desulfurization systems (Chen et al., 2014), the stricter control measures such as terminating
46 production in industries and construction as well as the odd and even number rule for vehicles
47 have been performed in megacities during the period of the red alert for haze and so on. These
48 actions have made tremendous effects to decline pollution levels of primary pollutants including
49 $\text{PM}_{2.5}$ (fine particulate matter with an aerodynamic diameter less than $2.5 \mu\text{m}$) in recent years (Li

50 et al., 2019). However, the serious pollution events still occurred in many areas of
51 Beijing-Tianjin-Hebei (BTH) region in December 2016 and January 2017 (Li et al., 2019). It has
52 been acknowledged that the severe haze pollution is mainly ascribed to stagnant meteorological
53 conditions with high atmospheric relative humidity (RH) and low mixed boundary layer height,
54 strong emissions of primary gaseous pollutants and rapid formation of secondary inorganic
55 aerosols (SIAs, the sum of sulfate, nitrate and ammonium), especially sulfate and nitrate (Cheng et
56 al., 2016;Guo et al., 2014;Huang et al., 2014). Some studies suggested that the contribution of
57 SIAs to PM_{2.5} was higher than 50% during the most serious haze days (Quan et al., 2014;Xu et al.,
58 2017;Zheng et al., 2015a).

59 Generally, atmospheric sulfate and nitrate are formed through the oxidations of the precursor
60 gases (SO₂ and NO₂) by oxidants (e.g. OH radical, O₃) via gas-phase, heterogeneous and
61 aqueous-phase reactions (Ravishankara, 1997;Wang et al., 2013;Yang et al., 2015). It should be
62 noted that the recent study proposed the remarkable emissions of primary sulfate from residential
63 coal combustion with the sulfur contents of coal in range of 0.81-1.88% in Xi'an (Dai et al., 2019),
64 but the primary emissions of sulfate could be neglected due to the extremely low sulfur content of
65 coal (0.26-0.34%) used prevalingly in the NCP (Du et al., 2016;Li et al., 2016). Atmospheric RH
66 is a key factor that facilitates the SIAs formation and aggravates the haze pollution (Wu et al.,
67 2019), and hence the secondary formations of sulfate and nitrate are simply considered to be
68 mainly via gas-phase reaction at relatively low atmospheric RH levels (RH<30%) and
69 heterogeneous reactions and aqueous-phase reactions at relatively high atmospheric RH levels
70 (RH>60%) (Li et al., 2017). However, their formation mechanisms at different atmospheric RH
71 levels still remain controversial and unclear (Cheng et al., 2016;Ge et al., 2017;Guo et al., 2017;Li

72 et al., 2018;Liu et al., 2017a;Wang et al., 2016;Yang et al., 2017). For example, the recent studies
73 proposed that atmospheric SO₂ oxidation by NO₂ dissolved in aqueous aerosol phases under the
74 extremely high atmospheric RH conditions played a dominant role in sulfate formation under
75 almost neutral aerosol solutions (a pH range of 5.4-7.0) during the serious pollution periods
76 (Cheng et al., 2016;Wang et al., 2018a;Wang et al., 2016). However, Liu et al. (2017a) and Guo et
77 al. (2017) found that the aerosol pH estimated by ISORROPIA-II model was moderately acidic (a
78 pH range of 3.0-4.9) and thus the pathway of SO₂ aqueous-phase oxidation by dissolved NO₂ was
79 unimportant during severe haze events in China. Additionally, although the pathway of N₂O₅
80 heterogeneous hydrolysis has been recognized as being responsible for the nocturnal formation of
81 NO₃⁻ under relatively high atmospheric RH conditions (Tham et al., 2018;Wang et al.,
82 2018b;Wang et al., 2018c), the effects of NO₂ gas-phase chemistry and NO₂ heterogeneous
83 chemistry on the diurnal formation of NO₃⁻ under moderate atmospheric RH conditions
84 (30%<RH<60%) have not yet been understood. Therefore, measurements of the species in PM_{2.5}
85 in different polluted cases during the wintertime are urgently needed to elucidate formation
86 pathways of sulfate and nitrate.

87 In this study, hourly filter samples of PM_{2.5} were collected continuously in Beijing during the
88 wintertime of 2016, and the pollution characteristics and formation mechanisms of sulfate and
89 nitrate in the PM_{2.5} samples were investigated comprehensively under different atmospheric RH
90 conditions in relation to gas-phase, heterogeneous and aqueous-phase chemistry.

91 **2. Materials and Methods**

92 **2.1. Sampling and analysis**

93 The sampling site was chosen on the rooftop (around 25 m above the ground) of a six-story

94 building in Research Center for Eco-Environmental Sciences, Chinese Academy of Sciences
95 (RCEES, CAS), which was located in the northwest of Beijing and had been described in detail by
96 our previous studies (Liu et al., 2016;Liu et al., 2017b). The location of the sampling site
97 ($40^{\circ}00'29.85''$ N, $116^{\circ}20'29.71''$ E) is presented in Figure S1. Hourly $PM_{2.5}$ samples were collected
98 on prebaked quartz fiber filters (90mm, Munktell) from January 7th to 23th of 2016 by
99 median-volume samplers (Laoying-2030) with a flow rate of 100 L min^{-1} . Water-soluble ions
100 (WSI), including Na^+ , NH_4^+ , Mg^{2+} , Ca^{2+} , K^+ , Cl^- , NO_2^- , NO_3^- and SO_4^{2-} , as well as carbon
101 components including organic carbon (OC) and element carbon (EC) in the filter samples were
102 analyzed by ion chromatography (Wayeal IC6200) and thermal optical carbon analyzer
103 (DRI-2001A), respectively (Liu et al., 2017b). Analysis relevant for quality assurance & quality
104 control (QA/QC) was presented in detail in section M1 of the Supplementary Information (SIs).
105 Atmospheric H_2O_2 and HONO were monitored by AL2021- H_2O_2 monitor (AERO laser, Germany)
106 and a set of double-wall glass stripping coil sampler coupled with ion chromatography (SC-IC),
107 respectively (Ye et al., 2018;Xue et al., 2019a;Xue et al., 2019b). More details about the
108 measurements of H_2O_2 and HONO were ascribed in section M2 of the SIs. Meteorological data,
109 including wind speed, wind direction, ambient temperature and RH, as well as air quality index
110 (AQI) derived by $PM_{2.5}$, SO_2 , NO_x , CO and O_3 were obtained from Beijing urban ecosystem
111 research station in RCEES, CAS (<http://www.bjurban.rcees.cas.cn/>).

112 **2.2. Aerosol liquid water contents and pH prediction by ISORROPIA-II model**

113 The ISORROPIA-II model was employed to calculate the equilibrium composition for
114 $Na^+-K^+-Ca^{2+}-Mg^{2+}-NH_4^+-Cl^- -NO_3^- -SO_4^{2-}-H_2O$ aerosol system, which is widely used in regional
115 and global atmospheric models and has been successfully applied in numerous studies for

116 predicting the physical state and composition of atmospheric inorganic aerosols (Fountoukis and
117 Nenes, 2007;Guo et al., 2015;Shi et al., 2017). It can be used in two modes: forward mode and
118 reverse mode. Forward mode calculates the equilibrium partitioning given the total concentrations
119 of gas and aerosol species, whereas reverse mode involves predicting the thermodynamic
120 compositions based only on the concentrations of aerosol components. Forward mode was
121 adopted in this study because reverse mode calculations have been verified to be not suitable to
122 characterize aerosol acidity (Guo et al., 2015;Hennigan et al., 2015;Murphy et al., 2017;Pathak et
123 al., 2004;Weber et al., 2016). The ISORROPIA-II model is available in “metastable” or “solid +
124 liquid” state solutions. Considering the relatively high RH during the sampling period, the
125 metastable state solution was selected in this study due to its better performance than the latter
126 (Bougiatioti et al., 2016;Guo et al., 2015;Liu et al., 2017a;Weber et al., 2016). Additionally,
127 although the gaseous HNO₃, H₂SO₄, HCl and NH₃ were not measured in this study, gas-phase
128 input with the exception of NH₃ has an insignificant impact on the aerosol liquid water contents
129 (ALWC) and pH calculation due to the lower concentrations of HNO₃, H₂SO₄ and HCl than NH₃
130 in the atmosphere (Ding et al., 2019;Guo et al., 2017). Based on the long-term measurement in the
131 winter of Beijing, an empirical equation between NO_x and NH₃ concentrations was derived from
132 the previous study (Meng et al., 2011), that is, $\text{NH}_3 (\text{ppb}) = 0.34 \times \text{NO}_x (\text{ppb}) + 0.63$, which was
133 employed for estimating the NH₃ concentration in this study. The predicted daily average
134 concentrations of NH₃ varied from 3.3 $\mu\text{g m}^{-3}$ to 36.9 $\mu\text{g m}^{-3}$, with a mean value of 16.6 $\mu\text{g m}^{-3}$
135 and a median value of 14.6 $\mu\text{g m}^{-3}$, which were in line with those (7.6-38.1 $\mu\text{g m}^{-3}$, 18.2 $\mu\text{g m}^{-3}$
136 and 16.2 $\mu\text{g m}^{-3}$ for the daily average concentrations, the mean value and the median value of NH₃,
137 respectively) during the winter of 2013 in Beijing in the previous study (Zhao et al., 2016).

138 Then, the aerosol pH could be calculated by the following equation:

$$139 \quad pH = -\log_{10} \frac{1000 \times H^+}{W}$$

140 where H^+ ($\mu\text{g m}^{-3}$) and W ($\mu\text{g m}^{-3}$) are the equilibrium particle hydrogen ion concentration
 141 and aerosol water contents, respectively, both of which could be output from ISORROPIA-II.

142 2.3. Production of sulfate in aqueous-phase reactions

143 The previous studies showed that there were six pathways of the aqueous-phase oxidation of
 144 SO_2 to the production of sulfate, i.e. H_2O_2 oxidation, O_3 oxidation, NO_2 oxidation, transition metal
 145 ions (TMI) + O_2 oxidation, methyl hydrogen peroxide (MHP) oxidation and peroxyacetic acid
 146 (PAA) oxidation (Cheng et al., 2016;Zheng et al., 2015a). Because some TMIs, such as Ti(III),
 147 V(III), Cr(III), Co(II), Ni(II), Cu(II) and Zn(II), displayed much less catalytic activities (Cheng et
 148 al., 2016), only Fe(III) and Mn(II) were considered in this study. In addition, due to the extremely
 149 low concentrations of MHP and PAA in the atmosphere, their contributions to the production of
 150 sulfate could be ignored (Zheng et al., 2015a). To investigate the formation mechanism of sulfate
 151 during the serious pollution episodes, the contributions of O_3 , H_2O_2 , NO_2 and Fe(III) + Mn(II) to
 152 the production of sulfate in aqueous-phase reactions were calculated by the formulas as follows
 153 (Cheng et al., 2016;Ibusuki and Takeuchi, 1987;Seinfeld and Pandis, 2006):

$$154 \quad -\left(\frac{d[S(IV)]}{dt}\right)_{\text{O}_3} = (k_0[\text{SO}_2 \cdot \text{H}_2\text{O}] + k_1[\text{HSO}_3^-] + k_2[\text{SO}_3^{2-}])[\text{O}_3(\text{aq})] \quad (\text{R1})$$

$$155 \quad -\left(\frac{d[S(IV)]}{dt}\right)_{\text{H}_2\text{O}_2} = \frac{k_3[H^+][\text{HSO}_3^-][\text{H}_2\text{O}_2(\text{aq})]}{1+K[H^+]} \quad (\text{R2})$$

$$156 \quad -\left(\frac{d[S(IV)]}{dt}\right)_{\text{Fe(III)+Mn(II)}} = k_4[H^+]^a[\text{Mn(II)}][\text{Fe(III)}][\text{S(IV)}] \quad (\text{R3})$$

$$157 \quad -\left(\frac{d[S(IV)]}{dt}\right)_{\text{NO}_2} = k_5[\text{NO}_2(\text{aq})][\text{S(IV)}] \quad (\text{R4})$$

158 where $k_0 = 2.4 \times 10^4 \text{ M}^{-1} \text{ s}^{-1}$, $k_1 = 3.7 \times 10^5 \text{ M}^{-1} \text{ s}^{-1}$, $k_2 = 1.5 \times 10^9 \text{ M}^{-1} \text{ s}^{-1}$, $k_3 = 7.45 \times 10^7 \text{ M}^{-1} \text{ s}^{-1}$, $K =$
 159 13 M^{-1} , $k_4 = 3.72 \times 10^7 \text{ M}^{-1} \text{ s}^{-1}$, $a = -0.74$ ($\text{pH} \leq 4.2$) or $k_4 = 2.51 \times 10^{13} \text{ M}^{-1} \text{ s}^{-1}$, $a = 0.67$ ($\text{pH} > 4.2$), and

160 $k_5 = (1.24-1.67) \times 10^7 \text{ M}^{-1} \text{ s}^{-1}$ ($5.3 \leq \text{pH} \leq 8.7$, the linear interpolated values were used for pH between
 161 5.3 and 8.7) at 298 K (Clifton et al., 1988); $[\text{O}_3(\text{aq})]$, $[\text{H}_2\text{O}_2(\text{aq})]$ and $[\text{NO}_2(\text{aq})]$ could be calculated by
 162 the Henry's constants which are $1.1 \times 10^{-2} \text{ M atm}^{-1}$, $1.0 \times 10^5 \text{ M atm}^{-1}$ and $1.0 \times 10^{-2} \text{ M atm}^{-1}$ at 298 K
 163 for O_3 , H_2O_2 and NO_2 respectively (Seinfeld and Pandis, 2006). As for $[\text{Fe(III)}]$ and $[\text{Mn(II)}]$, their
 164 concentrations entirely depended on the values of pH due to the precipitation equilibriums of
 165 Fe(OH)_3 and Mn(OH)_2 (Graedel and Weschler, 1981). Considering the aqueous-phase ionization
 166 equilibrium of SO_2 , the Henry's constants of HSO_3^- , SO_3^{2-} and S(IV) could be expressed by the
 167 equations as follows (Seinfeld and Pandis, 2006):

$$168 \quad H_{\text{HSO}_3^-}^* = H_{\text{SO}_2} \frac{K_{S1}}{[\text{H}^+]} \quad (\text{R5})$$

$$169 \quad H_{\text{SO}_3^{2-}}^* = H_{\text{SO}_2} \frac{K_{S1}K_{S2}}{[\text{H}^+]^2} \quad (\text{R6})$$

$$170 \quad H_{\text{S(IV)}}^* = H_{\text{SO}_2} \left(1 + \frac{K_{S1}}{[\text{H}^+]} + \frac{K_{S1}K_{S2}}{[\text{H}^+]^2} \right) \quad (\text{R7})$$

171 where $H_{\text{SO}_2} = 1.23 \text{ M atm}^{-1}$, $K_{S1} = 1.3 \times 10^{-2} \text{ M}$ and $K_{S2} = 6.6 \times 10^{-8} \text{ M}$ at 298 K. In addition, all
 172 of rate constants (k), Henry's constants (H) and ionization constants (K) are evidently influenced
 173 on the ambient temperature and are calibrated by the formulas as follows (Seinfeld and Pandis,
 174 2006):

$$175 \quad k(T) = k(T_0) e^{\left[-\frac{E}{R} \left(\frac{1}{T} - \frac{1}{T_0} \right) \right]} \quad (\text{R8})$$

$$176 \quad H(T) = H(T_0) e^{\left[-\frac{\Delta H}{R} \left(\frac{1}{T} - \frac{1}{T_0} \right) \right]} \quad (\text{R9})$$

$$177 \quad K(T) = K(T_0) e^{\left[-\frac{E}{R} \left(\frac{1}{T} - \frac{1}{T_0} \right) \right]} \quad (\text{R10})$$

178 where T is the ambient temperature, $T_0=298 \text{ K}$, both E/R and $\Delta H/R$ varied in the different
 179 equations and their values could be found in Cheng et al., (2016).

180 Furthermore, mass transport was also considered for multiphase reactions in different
 181 medium and across the interface in section M3 of the SIs.

182 **3. Results and Discussion**

183 **3.1. Variation characteristics of the species in PM_{2.5} and typical gaseous pollutants**

184 The concentrations of the species in PM_{2.5} and typical gaseous pollutants including NO₂, SO₂,
185 O₃, HONO and H₂O₂ as well as atmospheric RH are shown in Figure 1. The meteorological
186 parameters (wind speed, wind direction, ambient temperature and direct radiation (DR)) as well as
187 the concentrations of PM_{2.5} are displayed in Figure S2. During the sampling period, the
188 concentrations of the species in PM_{2.5} and typical gaseous pollutants varied similarly on a
189 timescale of hours with a distinct periodic cycle of 3-4 days, suggesting that meteorological
190 conditions played a vital role in accumulation and dispersion of atmospheric pollutants (Xu et al.,
191 2011;Zheng et al., 2015b). For example, the relatively high levels of PM_{2.5} (>100 µg m⁻³) usually
192 occurred under the relatively stable meteorological conditions with the low south wind speed (<2
193 m s⁻¹) and the high RH (>60%) which favored the accumulation of pollutants. Besides
194 meteorological conditions, the extremely high concentrations of the species in PM_{2.5} might be
195 mainly ascribed to strong emissions of primary pollutants and rapid formation of secondary
196 aerosols during the wintertime in Beijing.

197 The average concentrations of the species in PM_{2.5} and typical gaseous pollutants during
198 clean or slightly polluted (C&SP) episodes (PM_{2.5}<75 µg m⁻³), during polluted or heavy polluted
199 (P&HP) episodes (PM_{2.5}≥75 µg m⁻³) and during the whole sampling period are illustrated in Table
200 1. It is evident that the average concentrations of NO₃⁻, SO₄²⁻, NH₄⁺, OC and EC during P&HP
201 episodes were about a factor of 5.0, 4.1, 6.1, 3.6 and 3.2 greater than those during C&SP episodes,
202 respectively, indicating that the formations of SIAs were more efficient compared to other species
203 in PM_{2.5} during the serious pollution episodes. Given that the average concentrations of gaseous

204 precursors (NO_2 and SO_2) during P&HP episodes were approximately a factor of 2.0-2.2 greater
205 than those during C&SP episodes, the obviously higher elevation of NO_3^- and SO_4^{2-} implied that
206 the oxidations of NO_2 and SO_2 by the major atmospheric oxidizing agents (OH radicals, O_3 and
207 H_2O_2 etc.) might be greatly accelerated due to the relatively high concentrations of oxidants and
208 atmospheric RH during the serious pollution episodes (Figure 1). The average concentration of
209 H_2O_2 was found to be a factor of 1.7 greater during P&HP episodes than during C&SP episodes,
210 indicating that atmospheric H_2O_2 might contribute to the formation of SIAs especially sulfate
211 during the serious pollution episodes with high atmospheric RH, which will be discussed in Sect.
212 3.3.2. However, the obvious decrease in O_3 average concentration was observed during P&HP
213 episodes compared to C&SP episodes, which was mainly attributed to the relatively weak solar
214 radiation and the titration of NO during the serious pollution episodes (Ye et al., 2018). In addition,
215 the evidently higher average concentration of HONO during P&HP episodes than during C&SP
216 episodes might be also due to the relatively weak solar radiation as well as the heterogeneous
217 reaction of NO_2 on particle surfaces during the serious pollution episodes (Tong et al., 2016; Wang
218 et al., 2017).

219 **3.2. Three serious pollution cases during the sampling period**

220 Based on the transition from the clean to polluted periods, three haze cases were identified
221 during the sampling period (Figure 1 and Figure S2): from 13:00 on January 8th to 1:00 on January
222 11th (Case 1), from 14:00 on January 14th to 7:00 on January 17th (Case 2), and from 8:00 on
223 January 19th to 2:00 on January 22nd (Case 3). The serious pollution duration in the three cases
224 could last 1-3 days due to the differences of their formation mechanisms.

225 In Case 1, the variation trends of the concentrations of the species in $\text{PM}_{2.5}$, NO_2 , SO_2 ,

226 HONO and H₂O₂ were almost identical and exhibited three pollution peaks at night (Figure 1),
227 which might be ascribed to the possibility that the decrease of nocturnal mixed boundary layer
228 accelerated the pollutant accumulation (Bei et al., 2017;Zhong et al., 2019). Considering the
229 relatively low RH (15-40%) and wind speeds (<2 m s⁻¹) in Case 1 (Figure S2), primary emissions
230 around the sampling site were suspected to be a dominant source for the increase in the PM_{2.5}
231 concentrations. Further evidence is that the correlation between the concentrations of PM_{2.5} and
232 CO is better in Case 1 (R²=0.55) than in Case 2 and Case 3 (R²=0.20~0.52) (Figure S3). Identical
233 to Case 1, three obvious pollution peaks were also observed in Case 2 (Figure 1). The variation
234 trends of the concentrations of the species in PM_{2.5} and typical gaseous pollutants at the first peak
235 in Case 2 were found to be similar with those in Case 1, which were mainly attributed to their
236 similar formation mechanism. However, the evident decreases in NO_x and SO₂ were observed
237 when the concentrations of the species in PM_{2.5} were increasing and the atmospheric oxidation
238 pollutant (e.g. H₂O₂) concentration peaks were prior to others at the last two peaks in Case 2,
239 suggesting that secondary formation from gaseous precursors might be dominant for PM_{2.5}
240 pollution. The relatively high RH (50-80%) and the low south wind speeds (<2 m s⁻¹) in Case 2
241 (Figure S2) provided further evidence for the above speculation. In contrast to Case 1 and Case 2,
242 the relatively high south wind speeds (>3 m s⁻¹) (Figure S2) with the concentrations of the species
243 in PM_{2.5} and typical gaseous pollutants increasing slowly (Figure 1) at the beginning of Case 3
244 indicated that regional transportation might be responsible for the atmospheric species.
245 Subsequently, the concentrations of the species in PM_{2.5} remained relatively high when the
246 atmospheric RH lasted more than 60%, implying that secondary formation from gaseous
247 precursors dominated PM_{2.5} pollution during the late period of Case 3.

248 The average mass proportions of the species in PM_{2.5} in the three cases are illustrated in
249 Figure S4, the proportions of the primary species such as EC (10-13%), Cl⁻ (6-7%) and Na⁺ (4%)
250 in the three cases were almost identical, indicating that primary particle emissions were relatively
251 stable during the sampling period. However, the proportions of SIA in Case 2 (42%) and Case 3
252 (38%) were conspicuously greater than that in Case 1 (28%), further confirming that secondary
253 formation of inorganic ions (e.g. nitrate, sulfate) made a significant contribution to atmospheric
254 PM_{2.5} in Case 2 and Case 3.

255 3.3. Formation mechanism of nitrate and sulfate during serious pollution episodes

256 As for nitrate and sulfate in the three cases, the highest mass proportion (18%) of nitrate was
257 observed in Case 2, whereas the highest mass proportion (15%) of sulfate was found in Case 3
258 (Figure S4). Although the concentrations of SO₂ were obviously lower than the concentrations of
259 NO₂ in both Case 2 and Case 3 (Figure 1 and Table 1), the extremely high proportion of sulfate in
260 Case 3 might be ascribed to the long-lasting plateau of RH (Figure S2) because the aqueous-phase
261 reaction could accelerate the conversion of SO₂ to SO₄²⁻. To further investigate the pollution
262 characteristics of nitrate and sulfate during the serious pollution episodes, the relations between
263 NOR (NOR = NO₃⁻ / (NO₃⁻+NO₂)) as well as SOR (SOR = SO₄²⁻ / (SO₄²⁻+SO₂)) and RH are
264 shown in Figure 2. There were obvious differences in the variations of NOR and SOR under
265 different atmospheric RH conditions. The variation trends of NOR and SOR almost stayed the
266 same when atmospheric RH was below 30%, and then simultaneously increased with atmospheric
267 RH in the range of 30-60%. The enhanced gas-phase reaction and the heterogeneous reaction
268 involving aerosol liquid water might make a remarkable contribution to the elevation of NOR and
269 SOR, respectively, which were further discussed in the following section. Subsequently, the

270 variation trend of NOR slowly decreased whereas the variation trend of SOR significantly
271 increased when atmospheric RH was above 60%, which was very similar with the previous studies
272 (Sun et al., 2013;Zheng et al., 2015b). Considering that the heterogeneous reactions of NO₂ on
273 particle surface were dependent on atmospheric RH due to the competition of water for surface
274 reactive sites of particles (Ponczek et al., 2019), the slow reduction of NOR might be due to the
275 suppressed heterogeneous reaction of NO₂ to nitrate formation under high RH condition (Tang et
276 al., 2017), while the elevation of SOR revealed the dominant contribution of the aqueous-phase
277 reaction to sulfate formation.

278 **3.3.1. Formation mechanism of nitrate**

279 Atmospheric nitrate is considered to be mainly from NO₂ oxidation by OH radical in the gas
280 phase, heterogeneous uptake of NO₂ on the surface of particles and heterogeneous hydrolysis of
281 N₂O₅ on wet aerosols or chloride-containing aerosols (He et al., 2014;He et al., 2018;Nie et al.,
282 2014;Ravishankara, 1997;Wang et al., 2018b). Since atmospheric N₂O₅ is usually produced by the
283 reaction of NO₃ radical with NO₂ as well as both NO₃ radical and N₂O₅ are easily photolytic
284 during the daytime, the heterogeneous hydrolysis of N₂O₅ is a nighttime pathway for the
285 formation of atmospheric nitrate (He et al., 2018;Wang et al., 2018b). As shown in Figure 3a, the
286 mean values of NOR during the nighttime remarkably elevated with atmospheric RH increasing,
287 the disproportionation of NO₂ and the heterogeneous hydrolysis of N₂O₅ involving aerosol liquid
288 water were suspected to dominate the nocturnal formation of nitrate under high RH conditions
289 during the sampling period (Ma et al., 2017;Wang et al., 2018b;Li et al., 2018). However, the
290 productions of HONO and nitrate should be equal through the disproportionation of NO₂ (Ma et
291 al., 2017), which could not explain the wide gaps between the average concentrations of HONO

292 (about $6.5 \mu\text{g m}^{-3}$) and nitrate (about $20.1 \mu\text{g m}^{-3}$) observed at the nighttime under high RH
293 conditions during the sampling period. Thus, the disproportionation of NO_2 made insignificant
294 contribution to the nocturnal formation of nitrate under high RH conditions. Considering that
295 atmospheric NO_3 radical is mainly generated via the oxidation of NO_2 by O_3 , the relatively high
296 O_3 and NO_2 levels could be in favor of the formation of N_2O_5 during the nighttime (He et al.,
297 2018; Wang et al., 2018b), and hence the correlation between $[\text{NO}_2]^2 \times [\text{O}_3]$ and NOR can
298 represent roughly the contribution of the heterogeneous hydrolysis of N_2O_5 to atmospheric nitrate
299 at night. As shown in Figure 3b, although the variations of $[\text{NO}_2]^2 \times [\text{O}_3]$ at the nighttime
300 (18:00-7:00) were all positively correlated with NOR under the three different RH conditions,
301 their correlation under the $\text{RH} \geq 60\%$ condition ($R^2=0.552$) was significantly stronger than those
302 under the $\text{RH} < 60\%$ condition ($R^2 \leq 0.181$). It has been acknowledged that the correlation between
303 two species means the impact of changes in one species on another. The stronger the correlation is,
304 the greater the impact is. Therefore, the significantly stronger correlations between NOR and
305 $[\text{NO}_2]^2 \times [\text{O}_3]$ under the $\text{RH} \geq 60\%$ condition than under the $\text{RH} < 60\%$ condition revealed that the
306 heterogeneous hydrolysis of N_2O_5 made a remarkable contribution to atmospheric nitrate at the
307 nighttime under high RH condition. Additionally, the obviously lower slope of the correlation
308 between NOR and $[\text{NO}_2]^2 \times [\text{O}_3]$ under the $\text{RH} \geq 60\%$ condition (slope=11691) than under the
309 $\text{RH} < 60\%$ condition (slope ≥ 17399) (Figure 3b) also suggested that the formation of atmospheric
310 nitrate at the nighttime under high RH condition was more sensitive to the pathway of N_2O_5 .

311 However, the obvious increase in the mean values of NOR during the daytime (especially for
312 10:00-17:00) under the $30\% < \text{RH} < 60\%$ condition (Figure 3a) indicated that additional sources
313 rather than the heterogeneous hydrolysis of N_2O_5 were responsible for the formation of nitrate. To

314 explore the possible formation mechanisms of nitrate in this case, the daily variations of [Dust]
315 (the sum of Ca^{2+} and Mg^{2+}) \times $[\text{NO}_2]$ and $[\text{HONO}]$ (the main source of OH) \times [DR] \times $[\text{NO}_2]$,
316 which can represent roughly the heterogeneous reaction of NO_2 on the surface of mineral aerosols
317 and the gas-phase reaction of NO_2 with OH, are shown in Figure 3c and Figure 3d, respectively.
318 The mean values of $[\text{HONO}] \times [\text{DR}] \times [\text{NO}_2]$ during the daytime were found to be remarkably
319 greater under the $30\% < \text{RH} < 60\%$ condition than under the $\text{RH} \leq 30\%$ condition, whereas the mean
320 values of $[\text{Dust}] \times [\text{NO}_2]$ almost stayed the same under the two different RH conditions.
321 Considering the coincident trend of NOR and $[\text{HONO}] \times [\text{DR}] \times [\text{NO}_2]$ during the daytime
322 (10:00-17:00) under the $30\% < \text{RH} < 60\%$ condition, the gas-phase reaction of NO_2 with OH played
323 a key role in the diurnal formation of nitrate at moderate RH levels with the haze pollution
324 accumulating. It should be noted that the mean values of $[\text{HONO}] \times [\text{DR}] \times [\text{NO}_2]$ decreased
325 dramatically from 14:00 to 17:00 (Figure 3d), which was not responsible for the high mean values
326 of NOR at that time (Figure 3a). However, the slight increase in the mean values of $[\text{Dust}] \times [\text{NO}_2]$
327 after 14:00 was observed under the $30\% < \text{RH} < 60\%$ condition (Figure 3c) and hence the
328 heterogeneous reaction of NO_2 on the surface of mineral aerosols was suspected to contribute to
329 the diurnal formation of nitrate at that time under moderate RH condition.

330 **3.3.2. Formation mechanism of sulfate**

331 Atmospheric sulfate is principally from SO_2 oxidation pathway, including gas-phase
332 reactions with OH radical or stabilized Criegee intermediates, heterogeneous-phase reactions on
333 the surface of particles and aqueous-phase reactions with dissolved O_3 , NO_2 , H_2O_2 and organic
334 peroxides, as well as autoxidation catalyzed by TMI (Cheng et al., 2016; Li et al.,
335 2018; Ravishankara, 1997; Shao et al., 2019; Wang et al., 2016; Xue et al., 2016; Zhang et al., 2018).

336 As shown in Figure 4, similar to the daily variations of NOR, the mean values of SOR were found
337 to elevated remarkably under the $30\% < RH < 60\%$ condition compared to the $RH \leq 30\%$ condition,
338 especially during 14:00-22:00, which might be mainly ascribed to the enhanced gas-phase reaction
339 and the heterogeneous reaction of SO_2 involving aerosol liquid water under the relatively high RH
340 condition. The extremely high mean values of SOR during the whole day under the $RH \geq 60\%$
341 condition implied that aqueous oxidation of SO_2 dominated the formation of sulfate during the
342 severe pollution episodes, which was in line with previous studies (Zhang et al., 2018; Cheng et al.,
343 2016). A key factor that influenced the aqueous oxidation pathways for sulfate formation has been
344 considered to be the aerosol pH (Guo et al., 2017; Liu et al., 2017a), varying from 4.5 to 8.5 at
345 different atmospheric RH and sulfate levels during the sampling period (Figure 5a) on the basis of
346 the ISORROPIA-II model. Considering that the aqueous-phase chemistry of sulfate formation
347 usually occurs in severe haze events with relatively high atmospheric RH, the aerosol pH (4.5-5.3)
348 under the $RH \geq 60\%$ condition, which was lower than those (5.4-7.0) in the studies of Wang et al.,
349 (2016) and Cheng et al., (2016) but was slightly higher than those (3.0-4.9) in the studies of Liu et
350 al., (2017a) and Guo et al., (2017), was adopted for evaluating sulfate production in this study. In
351 addition, in terms of oxidants, the obvious increase in the average concentration of NO_2 (Figure 5b)
352 and the evident decrease in the average concentration of O_3 (Figure 5d) were observed with the
353 deterioration of $PM_{2.5}$ pollution. Furthermore, the average concentration of H_2O_2 was also found
354 to be extremely high (0.25 ppb) under the HP condition (Figure 5c) and was above 1 order of
355 magnitude higher than that (0.01 ppb) assumed by Cheng et al., (2016), which probably resulted in
356 the underestimation of the contribution of H_2O_2 to sulfate formation in the study of Cheng et al.,
357 (2016).

358 To further explore the contribution of H₂O₂ to sulfate production rate under the HP condition,
359 the parameters measured in this study (Table 2) and the same approach that was adopted by Cheng
360 et al., (2016) were used to calculate sulfate production. As shown in Figure 6, the relationships
361 between different aqueous oxidation pathways and aerosol pH in this study were found to be very
362 similar with those of Cheng et al., (2016). However, the contribution of H₂O₂ to sulfate production
363 rate was about a factor of 17 faster in this study (about 1.16 μg m⁻³ h⁻¹) than in the study (about
364 6.95×10⁻² μg m⁻³ h⁻¹) of Cheng et al., (2016), implying that the contribution of H₂O₂ to sulfate
365 formation was largely neglected. Furthermore, considering the aerosol pH calculated under the HP
366 condition during the sampling period, the oxidation pathway of NO₂ might play an insignificant
367 role in sulfate production rate (8.96×10⁻²-0.56 μg m⁻³ h⁻¹) and its importance proposed by the
368 previous studies (1.74-10.85 μg m⁻³ h⁻¹) was not necessarily expected.

369 4. Conclusion

370 Based on the comprehensive analysis of the pollution levels, the variation characteristics and
371 the formation mechanisms of the key species in PM_{2.5} and the typical gaseous pollutants during
372 the winter haze pollution periods in Beijing, three serious haze pollution cases were obtained
373 during the sampling period and the SIAs formations especially nitrate and sulfate were found to
374 make an evident contribution to atmospheric PM_{2.5} under the relatively high RH condition. The
375 significant correlation between [NO₂]² × [O₃] and NOR at night under the RH≥60% condition
376 indicated that the heterogeneous hydrolysis of N₂O₅ on wet aerosols was responsible for the
377 nocturnal formation of nitrate under extremely high RH conditions. The more coincident trend of
378 NOR and [HONO] × [DR] × [NO₂] than [Dust] × [NO₂] during the daytime under the
379 30%<RH<60% condition suggested that the gas-phase reaction of NO₂ with OH played a key role

380 in the diurnal formation of nitrate under moderate RH conditions. The extremely high mean values
381 of SOR during the whole day under the $RH \geq 60\%$ condition could be explained by the dominant
382 contribution of aqueous-phase reaction of SO_2 to atmospheric sulfate formation during the severe
383 pollution episodes. According to the parameters measured in this study and the same approach that
384 was adopted by Cheng et al., (2016), the oxidation pathway of H_2O_2 rather than NO_2 was found to
385 contribute greatly to atmospheric sulfate formation.

386 Our results revealed that the heavy pollution events in winter usually occurred with high
387 concentration levels of pollutants and oxidants as well as high liquid water contents of moderately
388 acidic aerosols in the NCP. Thus, emission controls of NO_x , SO_2 and VOCs especially under the
389 extremely high RH conditions are expected to reduce largely the pollution levels of nitrate and
390 sulfate in northern China and even in other pollution regions of China.

391

392 *Data availability.* Data are available from the corresponding author upon request
393 (yjmu@rcees.ac.cn)

394

395 *Author contributions.* YJM designed the experiments. PFL carried out the experiments and
396 prepared the manuscript. CY and CYX carried out the experiments. CLZ was involved in part of
397 the work. XS provided the meteorological data and trace gases in Beijing.

398

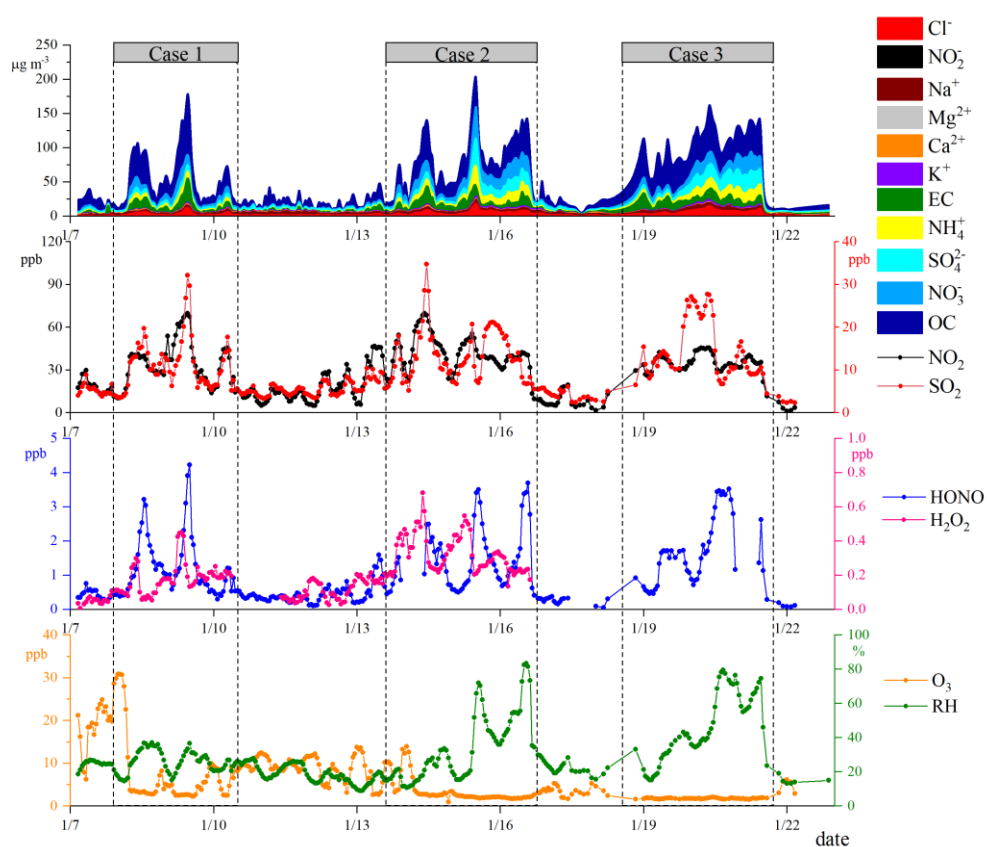
399 *Competing interests.* The authors declare that they have no conflict of interest.

400

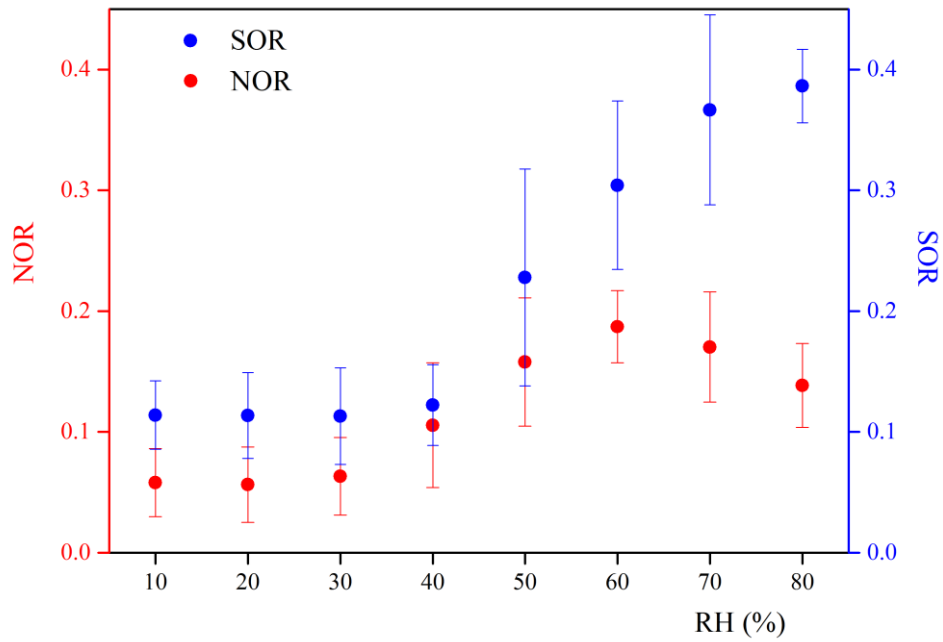
401 *Acknowledgement.* This work was supported by the National research program for Key issues in

402 air pollution control (No. DQGG0103, DQGG0209, DQGG0206), the National Natural Science
 403 Foundation of China (No. 91544211, 4127805, 41575121, 21707151), the National Key Research
 404 and Development Program of China (No. 2016YFC0202200, 2017YFC0209703,
 405 2017YFF0108301) and Key Laboratory of Atmospheric Chemistry, China Meteorological
 406 Administration (No. 2018B03).

407

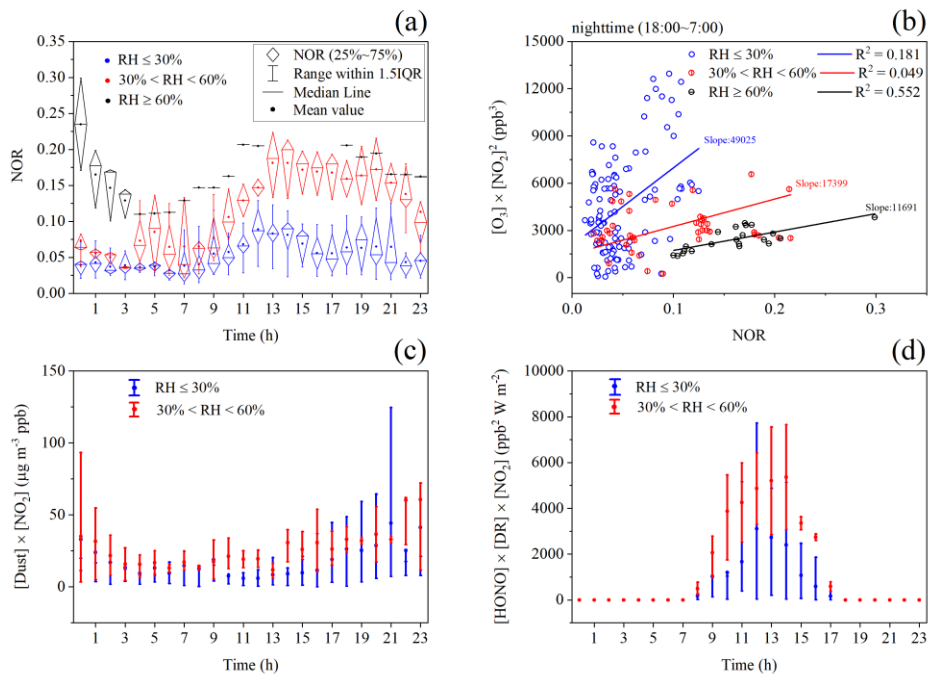


408 **Figure 1.** Time series of the species in PM_{2.5} and typical gaseous pollutants (NO₂, SO₂, O₃,
 409 HONO and H₂O₂) as well as atmospheric RH during the sampling period.
 410
 411



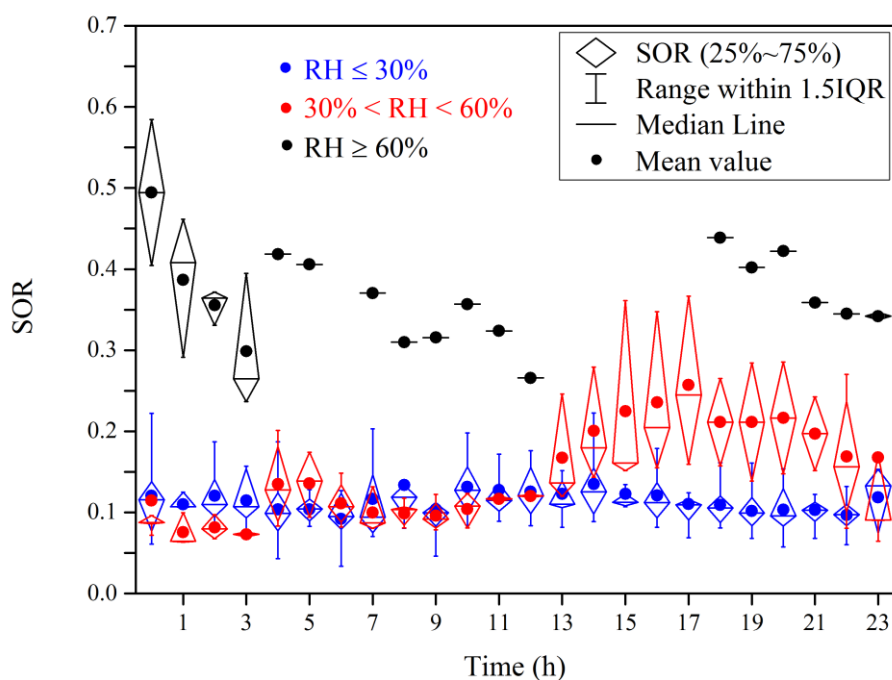
412
413
414

Figure 2. The relations between NOR as well as SOR and RH during the sampling period.



415
416
417
418
419

Figure 3. Daily variation of NOR (a), the correlation between NOR and $[\text{NO}_2]^2 \times [\text{O}_3]$ at the nighttime (18:00-7:00) (b), daily variations of $[\text{Dust}] \times [\text{NO}_2]$ and $[\text{HONO}] \times [\text{DR}] \times [\text{NO}_2]$ (c, d) under different atmospheric RH conditions during the sampling period.



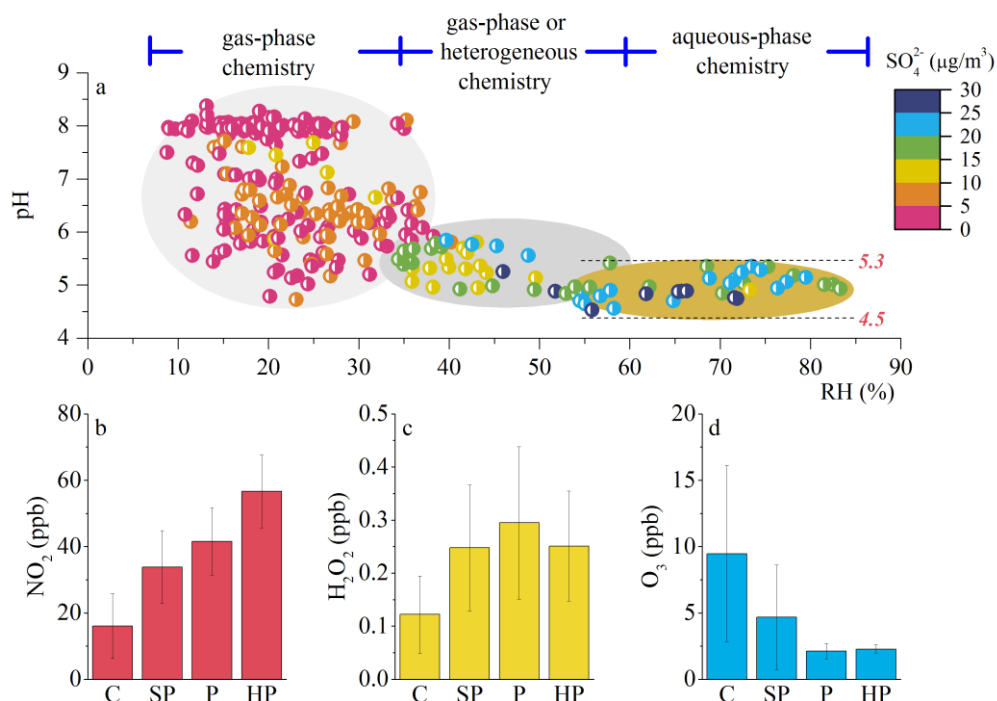
420

421

Figure 4. Daily variation of SOR under different atmospheric RH conditions during the sampling period.

422

423



424

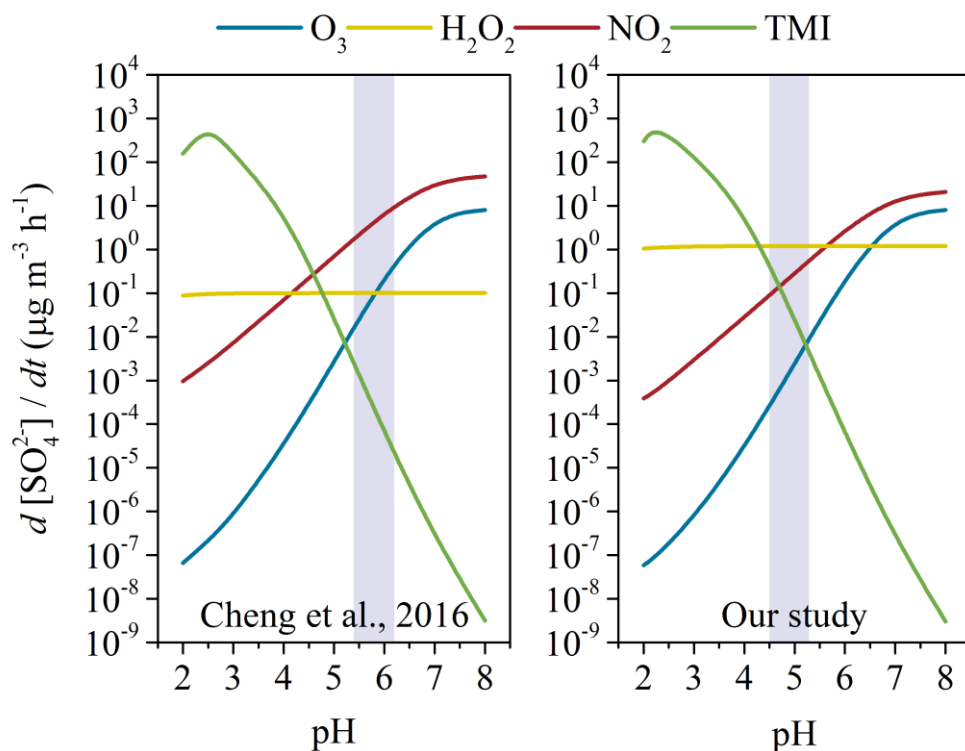
425

Figure 5. The correlations among aerosol pH, atmospheric RH and atmospheric SO_4^{2-} (a), the average concentrations of NO_2 , H_2O_2 and O_3 under different pollution conditions (clean (C), $\text{PM}_{2.5} < 35 \mu\text{g m}^{-3}$; slightly polluted (SP), $35 \mu\text{g m}^{-3} < \text{PM}_{2.5} < 75 \mu\text{g m}^{-3}$; polluted (P), $75 \mu\text{g m}^{-3} < \text{PM}_{2.5} < 150 \mu\text{g m}^{-3}$; heavily polluted (HP), $\text{PM}_{2.5} > 150 \mu\text{g m}^{-3}$).

427

428
429

$\text{m}^{-3} < \text{PM}_{2.5} < 150 \mu\text{g m}^{-3}$; heavy polluted (HP), $\text{PM}_{2.5} > 150 \mu\text{g m}^{-3}$) during the sampling period.



430
431
432
433
434
435
436

Figure 6. The comparison of aqueous-phase sulfate production by SO_2 oxidation under different aerosol pH conditions between in the study of Cheng et al., (2016) and in this study.

Table 1. The average concentrations of the species in $\text{PM}_{2.5}$ ($\mu\text{g m}^{-3}$) and typical gaseous pollutants (ppb) during C&SP episodes ($\text{PM}_{2.5} < 75 \mu\text{g m}^{-3}$), during P&HP episodes ($\text{PM}_{2.5} \geq 75 \mu\text{g m}^{-3}$) and during the whole sampling period.

species	during C&SP episodes (n=210)	during P&HP episodes (n=108)	total (n=318)
$\text{PM}_{2.5}$	30.00 ± 17.79	113.35 ± 28.10	58.31 ± 45.15
Na^+	2.88 ± 1.11	3.68 ± 1.19	3.15 ± 1.21
Mg^{2+}	0.05 ± 0.03	0.08 ± 0.06	0.06 ± 0.04
Ca^{2+}	0.52 ± 0.33	0.67 ± 0.48	0.58 ± 0.40
K^+	0.81 ± 0.42	1.84 ± 0.73	1.16 ± 0.73
NH_4^+	1.90 ± 1.90	11.52 ± 4.93	5.17 ± 5.62
SO_4^{2-}	3.64 ± 1.87	14.96 ± 7.80	7.47 ± 7.18
NO_3^-	3.44 ± 3.57	17.15 ± 7.36	8.10 ± 8.32
Cl^-	1.89 ± 1.20	7.35 ± 2.97	3.73 ± 3.26
NO_2^-	0.06 ± 0.08	0.06 ± 0.05	0.06 ± 0.07
OC	12.10 ± 9.25	43.34 ± 13.88	22.73 ± 18.48
EC	3.98 ± 3.42	12.69 ± 6.43	7.58 ± 6.51
NO_x	39.38 ± 35.25	107.71 ± 58.44	62.59 ± 54.98
NO_2	21.46 ± 13.04	42.81 ± 10.96	28.71 ± 15.98
SO_2	6.99 ± 3.64	15.70 ± 6.55	9.95 ± 6.35

O ₃	8.01 ± 6.35	2.13 ± 0.56	6.01 ± 5.87
HONO	0.60 ± 0.43	1.90 ± 0.97	1.01 ± 0.87
H ₂ O ₂	0.17 ± 0.11	0.29 ± 0.14	0.20 ± 0.13

437

438

439

Table 2. The comparisons for parameters of sulfate production rate calculations between in the study of Cheng et al., (2016) and in this work during the most polluted haze periods

Parameters	This study	Cheng et al., (2016)
NO ₂	57 ppb	66 ppb
H ₂ O ₂	0.25 ppb	0.01 ppb
O ₃	2 ppb	1 ppb
SO ₂	35 ppb	40 ppb
Fe(III) ^a	18 ng m ⁻³	18 ng m ⁻³
Mn(II) ^a	42 ng m ⁻³	42 ng m ⁻³
ALWC	146 µg m ⁻³	300 µg m ⁻³
Aerosol droplet radius (R) ^a	0.15 µm	0.15 µm
Temperature	270 K	271 K
pH	4.5-5.3	5.4-6.2

440

^a: both the concentrations of Fe(III) and Mn(II) and aerosol droplet radius were not measured in this study and were derived from Cheng et al., (2016).

441

442

443

References

444

Bei, N., Wu, J., Elser, M., Feng, T., Cao, J., El-Haddad, I., Li, X., Huang, R., Li, Z., Long, X., Xing, L., Zhao, S., Tie, X., Prévôt, A. S. H., and Li, G.: Impacts of meteorological uncertainties on the haze formation in Beijing–Tianjin–Hebei (BTH) during wintertime: a case study, *Atmospheric Chemistry and Physics*, 17, 14579-14591, 10.5194/acp-17-14579-2017, 2017.

448

Bougiatioti, A., Nikolaou, P., Stavroulas, I., Kouvarakis, G., Weber, R., Nenes, A., Kanakidou, M., and Mihalopoulos, N.: Particle water and pH in the eastern Mediterranean: source variability and implications for nutrient availability, *Atmospheric Chemistry and Physics*, 16, 4579-4591, 10.5194/acp-16-4579-2016, 2016.

452

Chan, C. K., and Yao, X.: Air pollution in mega cities in China, *Atmospheric Environment*, 42, 1-42, 10.1016/j.atmosenv.2007.09.003, 2008.

454

Chen, L. H., Sun, Y. Y., Wu, X. C., Zhang, Y. X., Zheng, C. H., Gao, X., and Cen, K.: Unit-based emission inventory and uncertainty assessment of coal-fired power plants, *Atmospheric Environment*, 99, 527-535, 10.1016/j.atmosenv.2014.10.023, 2014.

457

Cheng, Y., Zheng, G., Wei, C., Mu, Q., Zheng, B., Wang, Z., Gao, M., Zhang, Q., He, K., Carmichael, G., Pöschl, U., and Su, H.: Reactive nitrogen chemistry in aerosol water as a source of sulfate during haze events in China, *Science Advances*, 2, 1-11, 10.1126/sciadv.1601530, 2016.

460

Clifton, C. L., Altstein, N., and Huie, R. E.: Rate-constant for the reaction of NO₂ with sulfur(IV) over the pH range 5.3-13, *Environ. Sci. Technol.*, 22, 586-589, 10.1021/es00170a018, 1988.

462

Dai, Q., Bi, X., Song, W., Li, T., Liu, B., Ding, J., Xu, J., Song, C., Yang, N., Schulze, B. C., Zhang, Y., Feng, Y., and Hopke, P. K.: Residential coal combustion as a source of primary sulfate in Xi'an, China, *Atmospheric Environment*, 196, 66-76, 10.1016/j.atmosenv.2018.10.002, 2019.

465

Ding, J., Zhao, P., Su, J., Dong, Q., Du, X., and Zhang, Y.: Aerosol pH and its driving factors in Beijing,

466 Atmospheric Chemistry and Physics, 19, 7939-7954, 10.5194/acp-19-7939-2019, 2019.

467 Du, Q., Zhang, C., Mu, Y., Cheng, Y., Zhang, Y., Liu, C., Song, M., Tian, D., Liu, P., Liu, J., Xue, C.,
468 and Ye, C.: An important missing source of atmospheric carbonyl sulfide: Domestic coal combustion,
469 Geophysical Research Letters, 43, 8720-8727, 10.1002/2016gl070075, 2016.

470 Fountoukis, C., and Nenes, A.: ISORROPIA II: a computationally efficient thermodynamic equilibrium
471 model for K^+ - Ca^{2+} - Mg^{2+} - NH_4^+ - Na^+ - SO_4^{2-} - NO_3^- - Cl^- - H_2O aerosols, Atmospheric Chemistry and Physics,
472 7, 4639-4659, 2007.

473 Ge, X., He, Y., Sun, Y., Xu, J., Wang, J., Shen, Y., and Chen, M.: Characteristics and Formation
474 Mechanisms of Fine Particulate Nitrate in Typical Urban Areas in China, Atmosphere, 8, 62,
475 10.3390/atmos8030062, 2017.

476 Graedel, T. E., and Weschler, C. J.: Chemistry within aqueous atmospheric aerosols and raindrops,
477 Reviews of Geophysics, 19, 505-539, 10.1029/RG019i004p00505, 1981.

478 Guo, H., Xu, L., Bougiatioti, A., Cerully, K. M., Capps, S. L., Hite, J. R., Carlton, A. G., Lee, S. H.,
479 Bergin, M. H., Ng, N. L., Nenes, A., and Weber, R. J.: Fine-particle water and pH in the southeastern
480 United States, Atmospheric Chemistry and Physics, 15, 5211-5228, 10.5194/acp-15-5211-2015, 2015.

481 Guo, H., Weber, R. J., and Nenes, A.: High levels of ammonia do not raise fine particle pH sufficiently
482 to yield nitrogen oxide-dominated sulfate production, Scientific reports, 7, 12109,
483 10.1038/s41598-017-11704-0, 2017.

484 Guo, S., Hu, M., Zamora, M. L., Peng, J., Shang, D., Zheng, J., Du, Z., Wu, Z., Shao, M., Zeng, L.,
485 Molina, M. J., and Zhang, R.: Elucidating severe urban haze formation in China, Proceedings of the
486 National Academy of Sciences of the United States of America, 111, 17373-17378,
487 10.1073/pnas.1419604111, 2014.

488 He, H., Wang, Y., Ma, Q., Ma, J., Chu, B., Ji, D., Tang, G., Liu, C., Zhang, H., and Hao, J.: Mineral
489 dust and NO_x promote the conversion of SO_2 to sulfate in heavy pollution days, Scientific reports, 4,
490 1-5, 10.1038/srep04172, 2014.

491 He, P., Xie, Z., Chi, X., Yu, X., Fan, S., Kang, H., Liu, C., and Zhan, H.: Atmospheric $\Delta^{17}O(NO_3^-)$
492 reveals nocturnal chemistry dominates nitrate production in Beijing haze, Atmospheric Chemistry and
493 Physics, 18, 14465-14476, 10.5194/acp-18-14465-2018, 2018.

494 Hennigan, C. J., Izumi, J., Sullivan, A. P., Weber, R. J., and Nenes, A.: A critical evaluation of proxy
495 methods used to estimate the acidity of atmospheric particles, Atmospheric Chemistry and Physics, 15,
496 2775-2790, 10.5194/acp-15-2775-2015, 2015.

497 Huang, R. J., Zhang, Y., Bozzetti, C., Ho, K. F., Cao, J. J., Han, Y., Daellenbach, K. R., Slowik, J. G.,
498 Platt, S. M., Canonaco, F., Zotter, P., Wolf, R., Pieber, S. M., Bruns, E. A., Crippa, M., Ciarelli, G.,
499 Piazzalunga, A., Schwikowski, M., Abbaszade, G., Schnelle-Kreis, J., Zimmermann, R., An, Z., Szidat,
500 S., Baltensperger, U., El Haddad, I., and Prevot, A. S.: High secondary aerosol contribution to
501 particulate pollution during haze events in China, Nature, 514, 218-222, 10.1038/nature13774, 2014.

502 Ibusuki, T., and Takeuchi, K.: Sulfur-dioxide oxidation by oxygen catalyzed by mixtures of
503 manganese(II) and iron(III) in aqueous-solutions at environmental reaction conditions, Atmospheric
504 Environment, 21, 1555-1560, 10.1016/0004-6981(87)90317-9, 1987.

505 Li, G., Bei, N., Cao, J., Huang, R., Wu, J., Feng, T., Wang, Y., Liu, S., Zhang, Q., Tie, X., and Molina,
506 L. T.: A possible pathway for rapid growth of sulfate during haze days in China, Atmospheric
507 Chemistry and Physics, 17, 3301-3316, 10.5194/acp-17-3301-2017, 2017.

508 Li, J., Liao, H., Hu, J., and Li, N.: Severe particulate pollution days in China during 2013-2018 and the
509 associated typical weather patterns in Beijing-Tianjin-Hebei and the Yangtze River Delta regions,

510 Environ Pollut, 248, 74-81, 10.1016/j.envpol.2019.01.124, 2019.

511 Li, L., Hoffmann, M. R., and Colussi, A. J.: Role of nitrogen dioxide in the production of sulfate during
512 Chinese haze-aerosol episodes, *Environ Sci Technol*, 52, 2686-2693, 10.1021/acs.est.7b05222, 2018.

513 Li, Q., Li, X., Jiang, J., Duan, L., Ge, S., Zhang, Q., Deng, J., Wang, S., and Hao, J.: Semi-coke
514 briquettes: towards reducing emissions of primary PM_{2.5}, particulate carbon, and carbon monoxide
515 from household coal combustion in China, *Scientific reports*, 6, 1-10, 10.1038/srep19306, 2016.

516 Liu, M., Song, Y., Zhou, T., Xu, Z., Yan, C., Zheng, M., Wu, Z., Hu, M., Wu, Y., and Zhu, T.: Fine
517 particle pH during severe haze episodes in northern China, *Geophysical Research Letters*, 44, 1-9,
518 10.1002/2017GL073210, 2017a.

519 Liu, P., Zhang, C., Mu, Y., Liu, C., Xue, C., Ye, C., Liu, J., Zhang, Y., and Zhang, H.: The possible
520 contribution of the periodic emissions from farmers' activities in the North China Plain to atmospheric
521 water-soluble ions in Beijing, *Atmospheric Chemistry and Physics*, 16, 10097-10109,
522 10.5194/acp-16-10097-2016, 2016.

523 Liu, P., Zhang, C., Xue, C., Mu, Y., Liu, J., Zhang, Y., Tian, D., Ye, C., Zhang, H., and Guan, J.: The
524 contribution of residential coal combustion to atmospheric PM_{2.5} in northern China during winter,
525 *Atmospheric Chemistry and Physics*, 17, 11503-11520, 10.5194/acp-17-11503-2017, 2017b.

526 Ma, Q., Wang, T., Liu, C., He, H., Wang, Z., Wang, W., and Liang, Y.: SO₂ Initiates the efficient
527 conversion of NO₂ to HONO on MgO Surface, *Environ Sci Technol*, 51, 3767-3775,
528 10.1021/acs.est.6b05724, 2017.

529 Meng, Z. Y., Lin, W. L., Jiang, X. M., Yan, P., Wang, Y., Zhang, Y. M., Jia, X. F., and Yu, X. L.:
530 Characteristics of atmospheric ammonia over Beijing, China, *Atmospheric Chemistry and Physics*, 11,
531 6139-6151, 10.5194/acp-11-6139-2011, 2011.

532 Murphy, J. G., Gregoire, P. K., Tevlin, A. G., Wentworth, G. R., Ellis, R. A., Markovic, M. Z., and
533 VandenBoer, T. C.: Observational constraints on particle acidity using measurements and modelling of
534 particles and gases, *Faraday Discussions*, 200, 379-395, 10.1039/c7fd00086c, 2017.

535 Nie, W., Ding, A., Wang, T., Kerminen, V. M., George, C., Xue, L., Wang, W., Zhang, Q., Petaja, T., Qi,
536 X., Gao, X., Wang, X., Yang, X., Fu, C., and Kulmala, M.: Polluted dust promotes new particle
537 formation and growth, *Scientific reports*, 4, 1-6, 10.1038/srep06634, 2014.

538 Pathak, R. K., Louie, P. K. K., and Chan, C. K.: Characteristics of aerosol acidity in Hong kong,
539 *Atmospheric Environment*, 38, 2965-2974, 10.1016/j.atmosenv.2004.02.044, 2004.

540 Ponczek, M., Hayeck, N., Emmelin, C., and George, C.: Heterogeneous photochemistry of dicarboxylic
541 acids on mineral dust, *Atmospheric Environment*, 212, 262-271, 10.1016/j.atmosenv.2019.05.032,
542 2019.

543 Quan, J., Tie, X., Zhang, Q., Liu, Q., Li, X., Gao, Y., and Zhao, D.: Characteristics of heavy aerosol
544 pollution during the 2012–2013 winter in Beijing, China, *Atmospheric Environment*, 88, 83-89,
545 10.1016/j.atmosenv.2014.01.058, 2014.

546 Ravishankara, A.: Heterogeneous and multiphase chemistry in the troposphere, *Science*, 276,
547 1058-1065, 1997.

548 Seinfeld, J. H., and Pandis, S. N.: *Atmospheric Chemistry and Physics, from Air Pollution to Climate*
549 *Change*, Wiley, 429-443 pp., 2006.

550 Shao, J., Chen, Q., Wang, Y., Lu, X., He, P., Sun, Y., Shah, V., Martin, R. V., Philip, S., Song, S., Zhao,
551 Y., Xie, Z., Zhang, L., and Alexander, B.: Heterogeneous sulfate aerosol formation mechanisms during
552 wintertime Chinese haze events: air quality model assessment using observations of sulfate oxygen
553 isotopes in Beijing, *Atmospheric Chemistry and Physics*, 19, 6107-6123, 10.5194/acp-19-6107-2019,

554 2019.

555 Shi, G., Xu, J., Peng, X., Xiao, Z., Chen, K., Tian, Y., Guan, X., Feng, Y., Yu, H., Nenes, A., and
556 Russell, A. G.: pH of aerosols in a polluted atmosphere: source contributions to highly acidic aerosol,
557 *Environ Sci Technol*, 51, 4289-4296, 10.1021/acs.est.6b05736, 2017.

558 Sun, Y., Wang, Z., Fu, P., Jiang, Q., Yang, T., Li, J., and Ge, X.: The impact of relative humidity on
559 aerosol composition and evolution processes during wintertime in Beijing, China, *Atmospheric*
560 *Environment*, 77, 927-934, 10.1016/j.atmosenv.2013.06.019, 2013.

561 Tang, M., Huang, X., Lu, K., Ge, M., Li, Y., Cheng, P., Zhu, T., Ding, A., Zhang, Y., Gligorovski, S.,
562 Song, W., Ding, X., Bi, X., and Wang, X.: Heterogeneous reactions of mineral dust aerosol:
563 implications for tropospheric oxidation capacity, *Atmospheric Chemistry and Physics*, 17, 11727-11777,
564 10.5194/acp-17-11727-2017, 2017.

565 Tham, Y. J., Wang, Z., Li, Q., Wang, W., Wang, X., Lu, K., Ma, N., Yan, C., Kecorius, S., Wiedensohler,
566 A., Zhang, Y., and Wang, T.: Heterogeneous N₂O₅ uptake coefficient and production yield of ClNO₂ in
567 polluted northern China: roles of aerosol water content and chemical composition, *Atmospheric*
568 *Chemistry and Physics*, 18, 13155-13171, 10.5194/acp-18-13155-2018, 2018.

569 Tong, S. R., Hou, S. Q., Zhang, Y., Chu, B. W., Liu, Y. C., He, H., Zhao, P. S., and Ge, M. F.: Exploring
570 the nitrous acid (HONO) formation mechanism in winter Beijing: direct emissions and heterogeneous
571 production in urban and suburban areas, *Faraday Discussions*, 189, 213-230, 10.1039/c5fd00163c,
572 2016.

573 Wang, G., Zhang, R., Gomez, M. E., Yang, L., Levy Zamora, M., Hu, M., Lin, Y., Peng, J., Guo, S.,
574 Meng, J., Li, J., Cheng, C., Hu, T., Ren, Y., Wang, Y., Gao, J., Cao, J., An, Z., Zhou, W., Li, G., Wang,
575 J., Tian, P., Marrero-Ortiz, W., Secrest, J., Du, Z., Zheng, J., Shang, D., Zeng, L., Shao, M., Wang, W.,
576 Huang, Y., Wang, Y., Zhu, Y., Li, Y., Hu, J., Pan, B., Cai, L., Cheng, Y., Ji, Y., Zhang, F., Rosenfeld, D.,
577 Liss, P. S., Duce, R. A., Kolb, C. E., and Molina, M. J.: Persistent sulfate formation from London Fog
578 to Chinese haze, *Proceedings of the National Academy of Sciences of the United States of America*,
579 113, 13630-13635, 2016.

580 Wang, G., Zhang, F., Peng, J., Duan, L., Ji, Y., Marrero-Ortiz, W., Wang, J., Li, J., Wu, C., Cao, C.,
581 Wang, Y., Zheng, J., Secrest, J., Li, Y., Wang, Y., Li, H., Li, N., and Zhang, R.: Particle acidity and
582 sulfate production during severe haze events in China cannot be reliably inferred by assuming a
583 mixture of inorganic salts, *Atmospheric Chemistry and Physics*, 18, 10123-10132,
584 10.5194/acp-18-10123-2018, 2018a.

585 Wang, H., Lu, K., Chen, X., Zhu, Q., Wu, Z., Wu, Y., and Sun, K.: Fast particulate nitrate formation via
586 N₂O₅ uptake aloft in winter in Beijing, *Atmospheric Chemistry and Physics*, 18, 10483-10495,
587 10.5194/acp-18-10483-2018, 2018b.

588 Wang, H., Lu, K., Guo, S., Wu, Z., Shang, D., Tan, Z., Wang, Y., Le Breton, M., Lou, S., Tang, M., Wu,
589 Y., Zhu, W., Zheng, J., Zeng, L., Hallquist, M., Hu, M., and Zhang, Y.: Efficient N₂O₅ uptake and NO₃
590 oxidation in the outflow of urban Beijing, *Atmospheric Chemistry and Physics*, 18, 9705-9721,
591 10.5194/acp-18-9705-2018, 2018c.

592 Wang, J., Zhang, X., Guo, J., Wang, Z., and Zhang, M.: Observation of nitrous acid (HONO) in Beijing,
593 China: Seasonal variation, nocturnal formation and daytime budget, *The Science of the total*
594 *environment*, 587-588, 350-359, 10.1016/j.scitotenv.2017.02.159, 2017.

595 Wang, Y., Yao, L., Wang, L., Liu, Z., Ji, D., Tang, G., Zhang, J., Sun, Y., Hu, B., and Xin, J.:
596 Mechanism for the formation of the January 2013 heavy haze pollution episode over central and
597 eastern China, *Science China Earth Sciences*, 57, 14-25, 10.1007/s11430-013-4773-4, 2013.

598 Weber, R. J., Guo, H., Russell, A. G., and Nenes, A.: High aerosol acidity despite declining
599 atmospheric sulfate concentrations over the past 15 years, *Nature Geoscience*, 9, 282-285,
600 10.1038/ngeo2665, 2016.

601 Wu, J., Bei, N., Hu, B., Liu, S., Zhou, M., Wang, Q., Li, X., Liu, L., Feng, T., Liu, Z., Wang, Y., Cao, J.,
602 Tie, X., Wang, J., Molina, L. T., and Li, G.: Is water vapor a key player of the wintertime haze in North
603 China Plain?, *Atmospheric Chemistry and Physics*, 19, 8721-8739, 10.5194/acp-19-8721-2019, 2019.

604 Xu, L., Duan, F., He, K., Ma, Y., Zhu, L., Zheng, Y., Huang, T., Kimoto, T., Ma, T., Li, H., Ye, S., Yang,
605 S., Sun, Z., and Xu, B.: Characteristics of the secondary water-soluble ions in a typical autumn haze in
606 Beijing, *Environ Pollut*, 227, 296-305, 10.1016/j.envpol.2017.04.076, 2017.

607 Xu, W. Y., Zhao, C. S., Ran, L., Deng, Z. Z., Liu, P. F., Ma, N., Lin, W. L., Xu, X. B., Yan, P., He, X.,
608 Yu, J., Liang, W. D., and Chen, L. L.: Characteristics of pollutants and their correlation to
609 meteorological conditions at a suburban site in the North China Plain, *Atmospheric Chemistry and
610 Physics*, 11, 4353-4369, 10.5194/acp-11-4353-2011, 2011.

611 Xue, C., Ye, C., Ma, Z., Liu, P., Zhang, Y., Zhang, C., Tang, K., Zhang, W., Zhao, X., Wang, Y., Song,
612 M., Liu, J., Duan, J., Qin, M., Tong, S., Ge, M., and Mu, Y.: Development of stripping coil-ion
613 chromatograph method and intercomparison with CEAS and LOPAP to measure atmospheric HONO,
614 *The Science of the total environment*, 646, 187-195, 10.1016/j.scitotenv.2018.07.244, 2019a.

615 Xue, C., Ye, C., Zhang, Y., Ma, Z., Liu, P., Zhang, C., Zhao, X., Liu, J., and Mu, Y.: Development and
616 application of a twin open-top chambers method to measure soil HONO emission in the North China
617 Plain, *Sci. Total Environ.*, 659, 621-631, 10.1016/j.scitotenv.2018.12.245, 2019b.

618 Xue, J., Yuan, Z., Griffith, S. M., Yu, X., Lau, A. K., and Yu, J. Z.: Sulfate Formation Enhanced by a
619 Cocktail of High NO_x, SO₂, Particulate Matter, and Droplet pH during Haze-Fog Events in Megacities
620 in China: An Observation-Based Modeling Investigation, *Environ Sci Technol*, 50, 7325-7334,
621 10.1021/acs.est.6b00768, 2016.

622 Yang, T., Sun, Y., Zhang, W., Wang, Z., Liu, X., Fu, P., and Wang, X.: Evolutionary processes and
623 sources of high-nitrate haze episodes over Beijing, *Spring, J Environ Sci (China)*, 54, 142-151,
624 10.1016/j.jes.2016.04.024, 2017.

625 Yang, Y. R., Liu, X. G., Qu, Y., An, J. L., Jiang, R., Zhang, Y. H., Sun, Y. L., Wu, Z. J., Zhang, F., Xu,
626 W. Q., and Ma, Q. X.: Characteristics and formation mechanism of continuous hazes in China: a case
627 study during the autumn of 2014 in the North China Plain, *Atmospheric Chemistry and Physics*, 15,
628 8165-8178, 10.5194/acp-15-8165-2015, 2015.

629 Ye, C., Liu, P., Ma, Z., Xue, C., Zhang, C., Zhang, Y., Liu, J., Liu, C., Sun, X., and Mu, Y.: High H₂O₂
630 Concentrations Observed during Haze Periods during the Winter in Beijing: Importance of H₂O₂
631 Oxidation in Sulfate Formation, *Environmental Science & Technology Letters*, 5, 757-763,
632 10.1021/acs.estlett.8b00579, 2018.

633 Zhang, H., Chen, S., Zhong, J., Zhang, S., Zhang, Y., Zhang, X., Li, Z., and Zeng, X. C.: Formation of
634 aqueous-phase sulfate during the haze period in China: Kinetics and atmospheric implications,
635 *Atmospheric Environment*, 177, 93-99, 10.1016/j.atmosenv.2018.01.017, 2018.

636 Zhang, Q., He, K. B., and Huo, H.: Cleaning China's air, *Nature*, 484, 161-162, 2012.

637 Zhang, R., Wang, G., Guo, S., Zamora, M. L., Ying, Q., Lin, Y., Wang, W., Hu, M., and Wang, Y.:
638 Formation of urban fine particulate matter, *Chem Rev*, 115, 3803-3855, 10.1021/acs.chemrev.5b00067,
639 2015.

640 Zhao, M., Wang, S., Tan, J., Hua, Y., Wu, D., and Hao, J.: Variation of Urban Atmospheric Ammonia
641 Pollution and its Relation with PM_{2.5} Chemical Property in Winter of Beijing, China, *Aerosol and Air*

642 Quality Research, 16, 1390-1402, 10.4209/aaqr.2015.12.0699, 2016.
643 Zheng, B., Zhang, Q., Zhang, Y., He, K. B., Wang, K., Zheng, G. J., Duan, F. K., Ma, Y. L., and Kimoto,
644 T.: Heterogeneous chemistry: a mechanism missing in current models to explain secondary inorganic
645 aerosol formation during the January 2013 haze episode in North China, Atmospheric Chemistry and
646 Physics, 15, 2031-2049, 10.5194/acp-15-2031-2015, 2015a.
647 Zheng, G. J., Duan, F. K., Su, H., Ma, Y. L., Cheng, Y., Zheng, B., Zhang, Q., Huang, T., Kimoto, T.,
648 Chang, D., Pöschl, U., Cheng, Y. F., and He, K. B.: Exploring the severe winter haze in Beijing: the
649 impact of synoptic weather, regional transport and heterogeneous reactions, Atmospheric Chemistry
650 and Physics, 15, 2969-2983, 10.5194/acp-15-2969-2015, 2015b.
651 Zhong, J., Zhang, X., Wang, Y., Wang, J., Shen, X., Zhang, H., Wang, T., Xie, Z., Liu, C., Zhang, H.,
652 Zhao, T., Sun, J., Fan, S., Gao, Z., Li, Y., and Wang, L.: The two-way feedback mechanism between
653 unfavorable meteorological conditions and cumulative aerosol pollution in various haze regions of
654 China, Atmospheric Chemistry and Physics, 19, 3287-3306, 10.5194/acp-19-3287-2019, 2019.
655